Biophysical Journal Volume 70 April 1996 1628–1642

Energy Barrier Presented to Ions by the Vestibule of the Biological Membrane Channel

Matthew Hoyles,*‡ Serdar Kuyucak,‡ and Shin-Ho Chung*

*Protein Dynamics Unit, Department of Chemistry, and ‡Department of Theoretical Physics, Research School of Physical Sciences, Australian National University, Canberra, A.C.T. 0200, Australia

ABSTRACT The role of the vestibule in influencing the permeation of ions through biological ion channels is investigated. We derive analytical expressions for the electric potential satisfying Poisson's equation with prolate spheroidal boundary conditions. To allow more realistic geometries we devise an iterative method to calculate the electric potential arising from a fixed charge and an arbitrary dielectric boundary, and confirm that the analytical expressions and iterative method give similar potential values. We then investigate the size of the potential barrier presented to an ion by model vestibules of conical and catenary shapes. The height of the potential barrier increases steeply as an ion enters the vestibule and moves toward the constricted region of the channel. We show that the barrier presented by, for example, a 15° conical vestibule can be canceled by placing dipoles with a total moment of about 50 Debyes near the constricted region of the pore. The selectivity of cations and anions can result from the polarity of charge groups or the orientation of dipoles located near the constricted region of the channel.

INTRODUCTION

When an ion approaches the boundary between an aqueous electrolyte solution and a region of low dielectric strength, such as a protein wall or lipid bilayer, it experiences electrostatic repulsion due to induced charges in the dielectrics. If the boundary is an infinite plane, the electric potential due to it is equivalent to that from an imaginary image charge on the opposite side of the boundary from the real ion, but at the same distance; hence the term "image force" is used for this repulsion. The image charge is almost equal to the ion's charge; thus the repulsive force can be very large at small distances. Some other simple boundaries can be solved analytically using infinite series; we present the solution for a prolate spheroidal boundary in Appendix A. However, an analytical solution of the electric potential for more realistic channel geometries is not possible, and one has to use numerical techniques.

A cylindrical shape, used to model the gramicidin channel, has been a popular choice in the study of electrostatic potential barriers in channels (Parsegian, 1969; Levitt, 1978a,b; Jordan, 1981). By exploiting cylindrical symmetry, the two-dimensional problem of finding induced surface charges can be reduced to solving a set of one-dimensional integral equations, which requires less computational effort. As computational power is now less of a limiting factor, it has become possible to solve the original two-dimensional problem without imposing any symmetry restrictions and to determine potential barriers in more general channel geometries.

Received for publication 6 October 1995 and in final form 22 January 1996.

Address reprint requests to Dr. Shin-Ho Chung, Department of Chemistry, The Australian National University, Canberra, ACT 0200, Australia. Tel.: 61-6-249-2024; Fax: 61-6-247-2792; E-mail: shin-ho.chung@anu.edu.au.

0006-3495/96/04/1628/15 $2.00

Whereas the previous studies have been mainly concerned with the effects of an ion placed inside the membrane pore formed by a short peptide appropriate for the gramicidin channel (Jordan, 1981, 1982, 1983, 1984a,b, 1987; Levitt, 1978b), we address here a different problem: that of understanding the roles vestibules play in selecting ions and transporting them across the cell membrane. A common feature among ion-selective channels, ligand-gated or voltage-activated, are prominent vestibules, which extend about 60 Å above and 20 Å below the membrane surface. This feature is not shared by gramicidin channels. The transverse section of the acetylcholine channel has been deduced by electron microscope image reconstruction using crystallographic methods (Toyoshima and Unwin, 1988). Its vestibules appear to resemble catenaries.

We examined the influence of the dielectric boundary on an ion entering the vestibule, using an iterative method of computing the electric field at any point in two different dielectric media separated by an arbitrary boundary, for which Poisson's equation cannot be solved analytically. The method relies on the fact that the electric field of an ion in an electrolyte solution induces a surface charge density on the boundary. We divide the boundary into small sectors and calculate the charge density appearing on it due to the electric field from an ion in the electrolyte solution as well as that emanating from all other boundary sectors. After confirming that this numerical method of finding the electric potential agrees closely with that calculated with the analytical solution for a point charge outside a prolate spheroid, we compute the magnitudes of the repulsive force presented to an ion by vestibules, whose dimensions and shapes roughly correspond to that of the acetylcholine receptor channels (Unwin, 1989, 1995). We show that this repulsive force or energy barrier, unless it is canceled by dipoles located near the constricted region of the channel,

can severely attenuate the number of ions that can be transported across it.

METHOD

Potentials in dielectric media

We wish to solve Poisson's equation for general channel geometries, without imposing any symmetries either on the channel shape or on the position of ions. Clearly, this cannot be achieved using analytical methods, and one has to resort to iterative numerical techniques. Because the solution of Poisson's equation is unique for a closed boundary, convergence of results ensures that the solution found is the correct one.

Before applying the iterative technique we reduce the three-dimensional boundary value problem to an equivalent two-dimensional problem. Denoting the two regions by 1 (water, $\varepsilon_1 = 80$) and 2 (protein or lipid, $\varepsilon_2 = 2$), the potentials in each region satisfy Poisson's equation

$$\nabla^2\varphi_i = -\frac{\rho_i}{\varepsilon_0\varepsilon_i}, \quad i=1, 2, \tag{1}$$

where ρ_i and ε_i refer to the charge densities and the dielectric constants in the two regions. The constant ε_0 is the permittivity of free space. In addition, the potentials should satisfy the usual continuity conditions at the boundary

$$\varphi_1 = \varphi_2, \qquad \varepsilon_1\nabla\varphi_1 \cdot \hat{\mathbf{n}} = \varepsilon_2\nabla\varphi_2 \cdot \hat{\mathbf{n}}, \tag{2}$$

where $\hat{\mathbf{n}}$ is the unit normal to the surface. Equation 1 can be expressed in terms of the electric fields $\mathbf{E}$ as

$$\varepsilon_1\mathbf{E}_1 \cdot \hat{\mathbf{n}} = \varepsilon_2\mathbf{E}_2 \cdot \hat{\mathbf{n}}. \tag{3}$$

Following Levitt (1978a), we replace this system by an equivalent system of charges in a vacuum that produces the same electrical potential throughout space. The charge densities ρ_i are replaced by reduced charge densities ρ_i/ε_i. The discontinuity in the electric fields across the boundary can be represented by polarization charge density, σ, induced at the surface. Using an infinitesimal Gaussian pillbox across a surface area ΔS at position $\mathbf{r}$, the two are related by

$$(\mathbf{E}_1 - \mathbf{E}_2) \cdot \hat{\mathbf{n}} = \frac{\sigma}{\varepsilon_0}. \tag{4}$$

Thus the electric fields can be written as

$$\mathbf{E}_1 = \mathbf{E}_{ex} + \frac{\sigma}{2\varepsilon_0}\hat{\mathbf{n}}, \qquad \mathbf{E}_2 = \mathbf{E}_{ex} - \frac{\sigma}{2\varepsilon_0}\hat{\mathbf{n}}, \tag{5}$$

where $\mathbf{E}_{ex}$ is the part due to all the charges except those in ΔS. Eliminating $\mathbf{E}_2$ from Eqs. 3 and 4 and substituting $\mathbf{E}_1$ from Eq. 5, we obtain a relationship between the surface charge density and the external field

$$\sigma = 2\varepsilon_0\frac{\varepsilon_2 - \varepsilon_1}{\varepsilon_2 + \varepsilon_1}\mathbf{E}_{ex} \cdot \hat{\mathbf{n}}. \tag{6}$$

Here $\mathbf{E}_{ex} \cdot \hat{\mathbf{n}}$ is determined from the normal derivative of the external potential

$$\varphi_{ex}(\mathbf{r}) = \frac{1}{4\pi\varepsilon_0}\left[\sum_i \int \frac{\rho_i(\mathbf{r}')}{\varepsilon_i \mid \mathbf{r} - \mathbf{r}' \mid} dV' + \int_{\mathbf{r}'\neq\mathbf{r}} \frac{\sigma(\mathbf{r}')}{\mid \mathbf{r} - \mathbf{r}' \mid} dS'\right]. \tag{7}$$

Starting with an initial surface charge density of $\sigma_0(\mathbf{r}') = 0$, one can make an initial estimate of the potential at the boundary from Eq. 7. This potential is then fed into Eq. 6, and a new density $\sigma_1(\mathbf{r}')$ is obtained. Equations 6 and 7 are iterated until the results converge, that is, the difference between $\sigma^{(n-1)}$ and $\sigma^{(n)}$ is sufficiently small.

The potential energy of the ion is calculated from the expression

$$U(\mathbf{r}) = \frac{1}{2}\int \varphi(\mathbf{r})\rho_{free}(\mathbf{r})\, dV - U_{self}, \tag{8}$$

by numerical integration. Here U_{self} is the Born self-energy of the ion, and ρ_{free} refers to the charge density excluding the polarization charges induced on the boundary.

Iterative method of determining surface charges

This method is implemented as follows. The boundary is divided into smalls sectors of area ΔS_i, each represented by a point charge q_i at its center. First the charge density at each point is found using Eq. 6, based on the field from fixed charges (representing ions or dipoles). Then each point is assigned a charge equal to its charge density times the area it represents, $q_i = \sigma_i\Delta S_i$. The process is repeated, using both the fixed charges and the current estimate of the boundary charges, until the boundary charges converge.

Because the computation time grows with the square of the number of sectors, it is important to optimize the choice of sectional area. Two important considerations in this regard are, first, distance of the surface area to the external charges and, second, curvature of the area. At large distances from the external charges, the induced charge and the solid angle it subtends are small; hence one can use relatively larger areas for such sectors without introducing too much error. In contrast, because the relationship in Eq. 4 is strictly valid only for a flat surface, one must use relatively smaller areas in places where the curvature is high. The method we used for the correction of errors introduced by the curvature is detailed in the following section. In addition, the results of control runs indicate that each sector should have approximately equal vertical and horizontal spacing, and that although the spacing can be varied between different regions of the boundary, such variation must be done smoothly.

For convergence, we use the condition

$$\delta_i = \left| \frac{q_i^{(n)} - q_i^{(n-1)}}{q_{max}^{(n)}} \right|, \quad (9)$$

where $q_{max}^{(n)}$ is the largest charge in the nth iteration. The calculation is stopped when $\delta_i < 0.0001$ for all surface charges. The condition of Eq. 9 is preferred over the usual one with $q_i^{(n)}$ in the denominator, because it requires fewer iterations without loss in accuracy. The reason is that induced charges at large distances are very small, making them sensitive to small changes in other charges. Thus they take a long time to converge to the same level of accuracy as the larger charges. Yet the effects of these small charges on the calculated potentials are negligible. We carried out the computations using a supercomputer (Fujitsu VP 2200) with a vector processor, which is well suited to this type of algorithm.

The iterative method outlined above allows the electric potentials inside and outside of any arbitrarily shaped vestibule to be computed. Moreover, we are able to include the effects of an external electric field caused either by a potential difference applied across the membrane and channel or by the presence of monopoles or dipoles on the protein wall.

Curvature compensation

Because of the simplifying assumption that sectors are flat, and the induced charge on each sector is affected by the charges on all other sectors but not by their own charge, our method produces small but systematic errors when used on curved surfaces. It overestimates the potential near convex surfaces and underestimates that near concave surfaces. These errors can be reduced by spacing the surface points more closely, but there is a practical limit to the number of points that can be used, imposed by the available computer time and memory.

We use a method of compensating for curved sectors by incorporating an estimate of self-interaction into the polarizability of each sector. We assume that the charge density σ is constant across the sector, and that the electric field $\mathbf{E}$ and normal $\hat{\mathbf{n}}$ at the center of the sector are representative of the whole sector. The charge density is then given by

$$\sigma = P\mathbf{E} \cdot \hat{\mathbf{n}}, \quad (10)$$

where

$$P = 2\varepsilon_0 \frac{\varepsilon_2 - \varepsilon_1}{\varepsilon_2 + \varepsilon_1} \quad (11)$$

is the polarizability of the boundary. The electric field at the center of the sector breaks into two components: the external electric field $\mathbf{E}_{ext}$ from other sectors and fixed charges, and the electric field of self-interaction $\mathbf{E}_{self}$ from the other points of the sector. Hence

$$\sigma = P\mathbf{E}_{ext} \cdot \hat{\mathbf{n}} + P\mathbf{E}_{self} \cdot \hat{\mathbf{n}} \quad (12)$$

$$= \sigma_{ext} + \sigma_{self}, \quad (13)$$

where σ_{ext} is the charge density due to the external field, and σ_{self} is the charge density due to self-interaction. Because we assume that the charge density is constant across the sector, σ_{self} is directly proportional to σ. The constant of proportionality, which we call Q, depends only on the shape and size of the sector and the polarizability of the boundary, not on the external field. So we have

$$\sigma = \sigma_{ext} + Q\sigma \quad (14)$$

and

$$\sigma = \frac{1}{1 - Q} \sigma_{ext}. \quad (15)$$

We now define the modified polarizability P' so that it generates the full surface charge density from the external field alone

$$\sigma = P'\mathbf{E}_{ext} \cdot \hat{\mathbf{n}}, \quad (16)$$

then from Eq. 15

$$P'\mathbf{E}_{ext} \cdot \hat{\mathbf{n}} = \frac{1}{1 - Q} P\mathbf{E}_{ext} \cdot \hat{\mathbf{n}} \quad (17)$$

$$P' = \frac{1}{1 - Q} P. \quad (18)$$

By precalculating Q and modifying the polarizability of each sector we can compensate for curved sectors without modifying the iterative algorithm.

Validation of the iterative method

To test the validity of the iterative method, we compared the results with those obtained from an exact analytical solution. For this purpose, we chose the prolate spheroid boundary with an axis ratio of 5:1 and length of 100 Å, which approximately represents one globular channel protein. The analytical solutions for an ion outside this boundary are presented in Appendix A.

For the numerical calculations, we divided the spheroid vertically into rings with equal spacing Δt in parameter t, where the cross section of the spheroid is described by

$$x = a \cos t, \qquad y = b \sin t. \quad (19)$$

We used values of 10 Å for a, 50 Å for b, and 0.05 for Δt. The spacing varies from $a\Delta t$ at $(0, b)$ to $b\Delta t$ at $(a, 0)$; note that the spacing is smallest where the curvature is greatest. Each ring is divided horizontally into equal segments with arc length approximately equal to the vertical spacing for that ring.

We examined the potential of an ion moving past a single spheroid. Fig. 1 compares the exact and numerical results for the potential energy of the ion as it moves parallel to the spheroid's symmetry axis. At its closest approach the ion was 4.14 Å away from the surface of the spheroid. The potential energy calculated from the analytical solution given in Eq. 26 is shown as a solid line in Fig. 1 *a*.

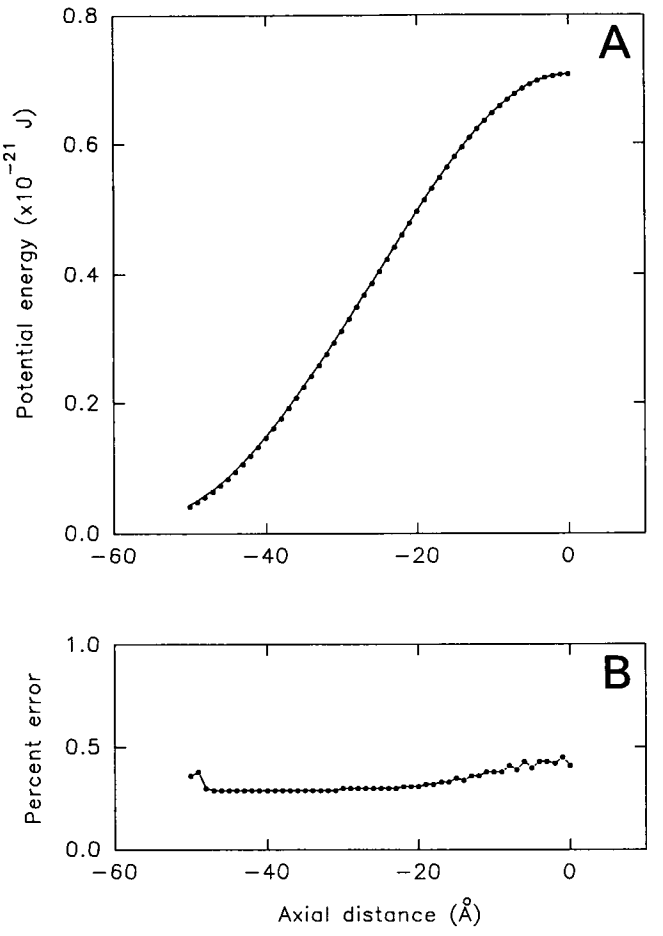

FIGURE 1 Comparison between the analytical solution and the iterative method. A cation is moved parallel to and 14.14 Å away from the major axis of a prolate spheroid that is 100 Å long and 20 Å in diameter at its widest section. At its closest approach the ion is 4.14 Å from the surface of the spheroid. Only the first half of the trajectory of the ion is shown, from the apex of the prolate (labeled as −50 Å) to its middle (labeled as 0 Å). (*a*) The energy barrier presented by the spheroid is plotted against the ion's position along its trajectory. The values computed from the analytical solution (*solid line*) using the equations given in the Appendix are superimposed on values calculated using the iterative method (*filled circles*). (*b*) The fractional error, calculated by dividing the difference between the analytical and numerical values by the analytical value at each location of the ion, is plotted against the position of the ion along its trajectory. The maximum error is about 0.5%.

Superimposed on this is the potential energy calculated by using the iterative method (*filled circles*). The values derived from the iterative method differed at most by 0.5% from those obtained from the analytical solution. The fractional error is given in Fig. 1 *b*.

A simple model for channels

One can make a simple model of a channel by putting four or five prolate spheroids together as suggested by Unwin (1989). Approximate analytic solutions for such a channel can be obtained by superposing the single spheroid solutions given in Appendix A. Comparison with the numerical results, however, shows that these approximate solutions underestimate the potential by up to a factor of 2 because of the neglect of interactions among the induced charges on different spheroids. Because there is no advantage (in the form of analytical solutions) to be gained from the use of a spheroidal channel, we prefer a simpler geometry, similar to an hourglass or bicone, which simplifies the computations.

We form the channel surface by rotating the closed curve around the symmetry z axis. An example of one such biconical channel is shown in Fig. 2. The biconical channels have a cylindrical neck region of length 10 Å and radius 4 Å, conical vestibules with a side length of 36 Å and an angle of 10° to 90° to vertical, annular top and bottom sections with a length of 10 Å, and a cylindrical side section. We connect these sections with curved corners to keep the surface smooth, as suggested by Jordan (1982). The inside corners, between the neck, the vestibules, and the top and bottom, have a radius of 5 Å. The outside corners between top, side, and bottom have a radius of 10 Å. The vestibules of catenary channels are formed by rotating a section of catenary; otherwise they are the same as biconical channels (see Fig. 4 *a*).

We place boundary points for channels by dividing the boundary vertically into rings, and each ring horizontally into equal segments. We keep the angle of horizontal spacing the same for all rings. This means that the spacing gets larger in proportion to the radius and that segments in adjacent rings line up vertically. We keep the vertical spacing between rings approximately equal to the horizontal spacing between segments in those rings. We used a horizontal angular spacing of 15° in the simulations, yielding a

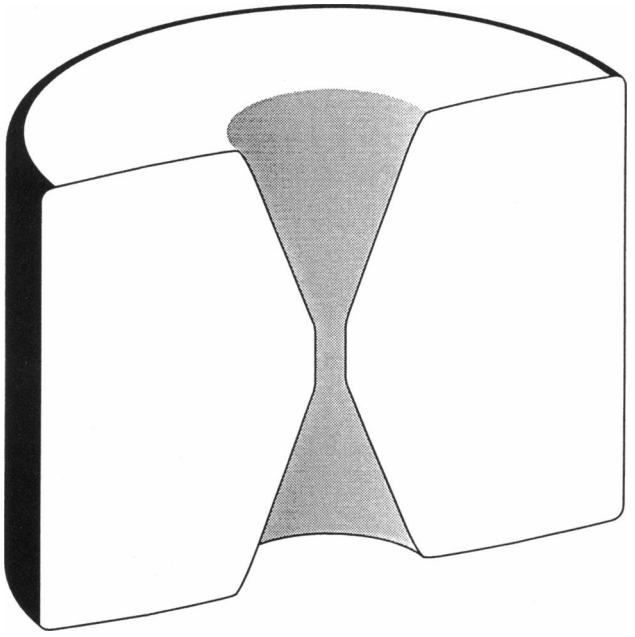

FIGURE 2 A transverse section of a 15° biconical channel. The surface of the model channel is generated by rotating the closed curve illustrated in Fig. 3 *a* along its symmetry axis. The dimensions of the two conical vestibules and the constricted segment are given in the text.

sector size that varies from 1 Å at the neck region to 10 Å at the back of the channel (see Fig. 3 *a*). Typically, a channel surface was divided into about 1600 sectors. The number of floating point operations needed to construct a profile of energy barrier was on the order of 10^{10}.

Simplifying assumptions

To make the determination of electrostatic potentials in the model channel computationally tractable, we make the following simplifying assumptions. First, ions outside the channel vestibule have a negligible effect on the potential energy of the ion inside of the vestibule. This is a reasonable approximation, because the induced charge on the boundary due to an ion at the position r from it decreases as $1/r^2$ (see Fig. 6 *b*; Jordan et al., 1989). At typical biological concentrations (140 mM) there are about 400 water molecules per ion. Each of two 15° conical vestibules in the model channel shown in Fig. 2 contains 400 water molecules. Thus, on average there is only one ion in such a vestibule. Furthermore, we limit our discussion of channel potentials here to only one kind of ion, because all known biological ion channels are permeable only to anions or cations, not both. The general case of multiple ions of both kinds will be the subject of a future paper in which Brownian dynamics will be used in simulating the motion of ions.

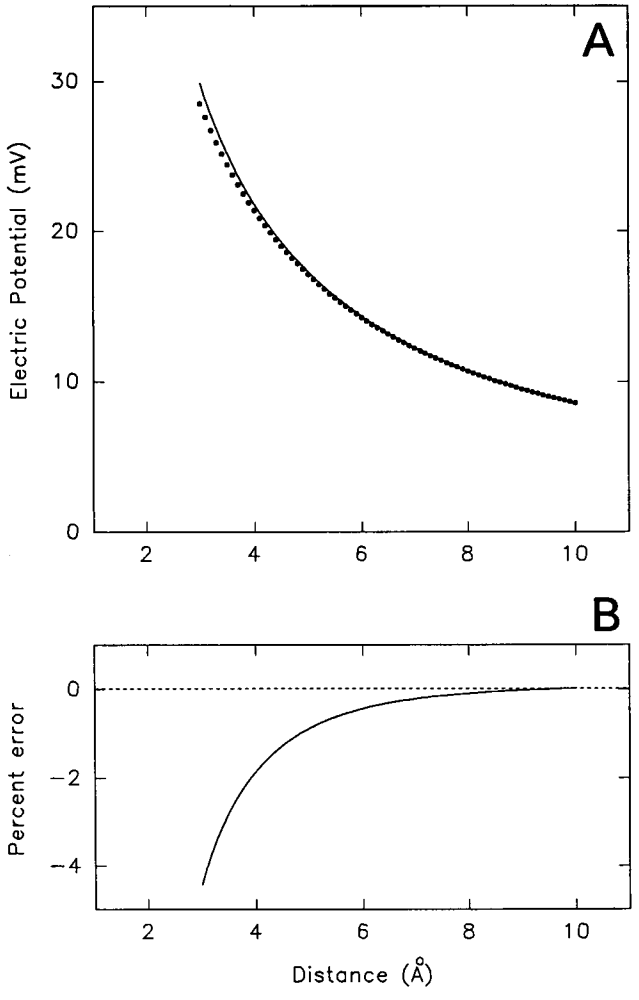

FIGURE 3 The magnitude of error introduced by ignoring the intermediate dielectric layer at the protein-water interface. In these figures, the thickness and dielectric constant of the intermediate layer are assumed to be 2 Å and 41, respectively. (*a*) Electric potentials are plotted as a function of the distance from the boundary. The distance is measured from the center of the intermediate layer. The dotted line is derived from the boundary of the protein-water interface, with no intermediate dielectric layer. Superimposed on this is a solid line calculated from a boundary that has a thin intermediate layer. (*b*) The fractional error, calculated by dividing the difference between the two potential values at each distance by the value from the boundary with the intermediate layer, is plotted against the distance of the ion from the center of the intermediate layer. The fractional error introduced by ignoring the intermediate layer when the ion is 2 Å from the interface is about 4%.

Second, we assume that the dielectric constant changes sharply at the protein-water boundary, from 2 to 80. Because dipolar or charged groups at the interface are likely to be realigned in the presence of a permeant ion, there will be a thin boundary layer with a dielectric constant intermediate between those of protein and water. To ascertain the magnitude of errors introduced by ignoring the intermediate dielectric region, we obtained an analytical expression for the potential resulting from a point charge near three infinite slabs having different dielectric constants. Numerical examples of the analytical solutions of this boundary-value problem, given in Appendix B, are illustrated in Fig. 3. A plot of electric potentials against the distance from the interface, calculated from Eq. 38, reveals that a small but systematic error is introduced when the intermediate layer is ignored (Fig. 3 *a*), but the fractional error decreases with increasing distance (Fig. 3 *b*). In these calculations, we took the thickness t and the dielectric constant ε_2 of the intermediate layer to be 2 Å and 41, respectively. At 2 Å from the interface, for example, the magnitude of error introduced by assuming an abrupt change in the dielectric constant at the interface is 4%. At 4 Å, the difference between the two- and three-layer interfaces becomes less than 1%. We thus conclude that the sharp boundary assumption introduces only negligibly small errors.

Finally, the results described here are macroscopic approximations, which are valid in regions that are large compared to the diameters of ions and water molecules. The idealizations implicitly assumed in electrostatic equations cannot be justifiably extended to the neighborhood of the constricted region of channel, in which the orientation of water molecules must be severely constrained. A proper treatment of ionic motion in the neck region of biological channels or in the gramicidin channel requires a microscopic approach, such as molecular dynamics calculations (see, for example, Roux and Karplus, 1991).

RESULTS

Repulsive force on an ion

As an ion moves into the vestibule, it induces charges that pose an energy barrier that impedes its passage across the

channel. We calculate the size of this barrier using the iterative method. The usual convention of zero potential energy at an infinite distance from the channel is adopted throughout. This results in a small initial potential energy of 3×10^{-22} J (or 2% of the energy at 0 Å) for the 15° bicone at $z = -50$ Å. We use dielectric constants of 80 for water and 2 for protein or membrane. In general we assume that we are dealing with a cationic channel and that the permeating ion is a monovalent positive ion.

As illustrated in Fig. 4 for a biconical channel, the potential barrier and repulsive force increase steadily as the ion moves from the entrance of the cone to the narrow constricted region. The narrow transmembrane segment is 4 Å in radius, and the wall of the conical vestibule is inclined 15° from the horizontal z axis, extending 38 Å beyond the constricted region. At the entrance of the constricted region, labeled as 0 Å in Fig. 4 *a*, the height of the potential barrier is 1.7×10^{-20} J, and the z component of the repulsive force is 6×10^{-12} N. For reasons stated previously and repeated in the Discussion, we have not tabulated here or in subsequent figures the barrier height or repulsive force on the ion inside the constricted region.

We have ascertained that the shape and magnitude of the potential barrier in a catenary vestibule are similar to those of a conical vestibule. In Fig. 5 *a* we show the cross section of a channel with catenary vestibules, like those visible in the electron microscopic picture of the acetylcholine chan-

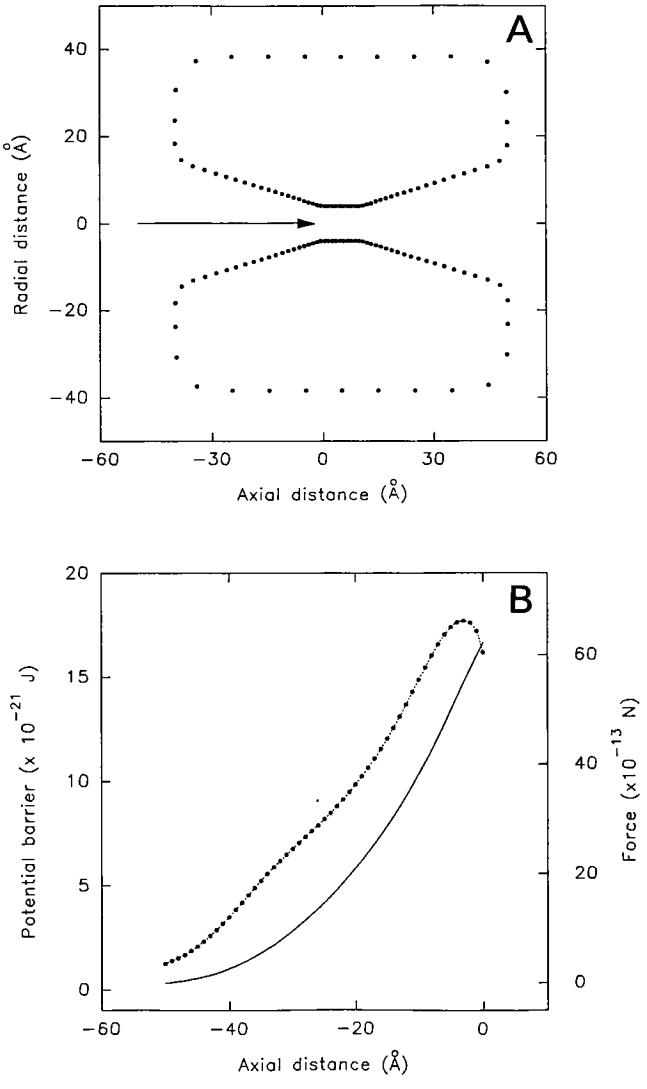

FIGURE 4 Potential barrier and repulsive force in a 15° conical vestibule. (*a*) The two closed curves outlined by dots are rotated along the (horizontal) symmetry axis to generate the surface of the model channel. The spacing of the dots represents the sizes of the sectors on the channel surface used for calculating induced surface charges. Note that the size of the sectors at the outer rim of the channel is large compared to that near the narrow region. The ion is assumed to move along the z axis, as indicated by the arrow. (*b*) The potential barrier (*solid line*) and repulsive force (*filled circles*) at each location along the ion's trajectory are shown.

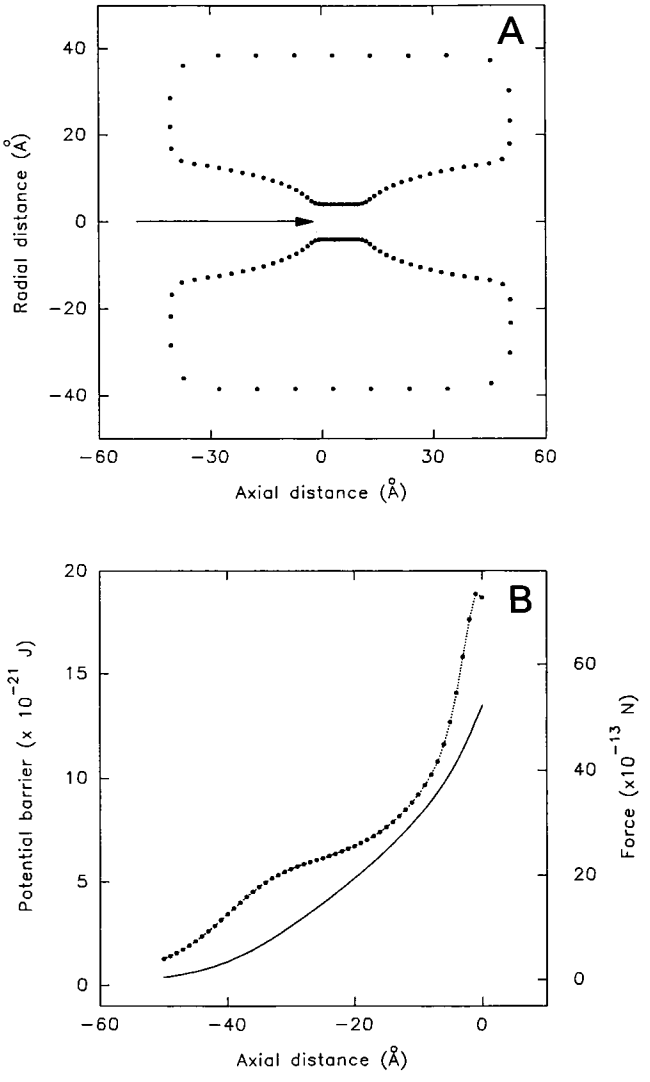

FIGURE 5 Potential barrier and repulsive force in a catenary channel. (*a*) To approximate the shape of the acetylcholine receptor channel, vestibules at each side of the membrane are constructed using a hyperbolic cosine function. The trajectory of the ion along the symmetry axis is shown with an arrow. (*b*) The potential barrier (*solid line*) and repulsive force (*filled circles*) at each location along the ion's trajectory are shown.

nel given by Toyoshima and Unwin (1988). The vestibule is generated by a hyperbolic cosine function, $y = a \cosh x/a$, where a = 4.75 Å. The radius of the entrance of the vestibule is fixed at 15 Å; in length and width of vestibules this channel is very similar to the 15° biconical channel (see Fig. 4 *a*). The maximum height of the energy barrier obtained from this channel, shown in Fig. 5 *b*, is 20% lower than that from the 15° biconical channel (cf. Fig. 4 *b*); it is nearly equal to a 20° biconical channel (see later). The shape of the repulsive force the ion encounters as it traverses toward the neck region is slightly different from that obtained from the biconical channel, rising first slowly and then sharply as it approaches the maximum. Because the conical and catenary vestibules give qualitatively similar potential profiles, all of the subsequent results we illustrate are derived from the conical vestibule. The same qualitative conclusions can be drawn from the results of simulations on the catenary vestibule.

Induced surface charges

Because the polarity of the induced charges on the protein wall is the same as that of the ion, the predominant force on the ion is a coulomb repulsion. In Fig. 6 *a*, the pattern of induced surface charges on a biconical channel wall at a fixed position of the ion is shown. These are the surface charges from the equivalent system described above. The ion is on the central axis of a 15° bicone, midway between the entrance of the vestibule and the constricted region of the pore, as indicated with an asterisk in the inset. Because each segment on a ring contributes equally to the potential energy, we show charge density per unit length. The magnitude of induced positive charges, expressed in units of C m^{-1}, is maximum at about the closest distance from the ion. They are distributed mainly on the walls of the cone and, to a lesser extent, on the wall of the constricted region of the pore. The induced counter-charges, not shown in Fig. 6 *a*, are located on the outer edge of the channel. The induced positive and negative charges computed with our numerical method approximately balance each other: the magnitude of the sum of negative charges exceeds the sum of positive charges by 2%. This small imbalance is presumably due to the much larger sectional areas used on the outer edge of the channel, where the negative charges are located.

The way the magnitude and spatial distribution of induced charges change as the ion moves toward the constricted region is displayed in Fig. 6 *b* as a three-dimensional graph. For each graph (which represents a fixed position of the ion), the surface charge per unit of z axis length on thin rings of the biconical wall are computed, and these values are plotted against the z axis. The area under each curve gives the total induced charge on the channel wall, which is seen to grow rapidly as the ion moves in.

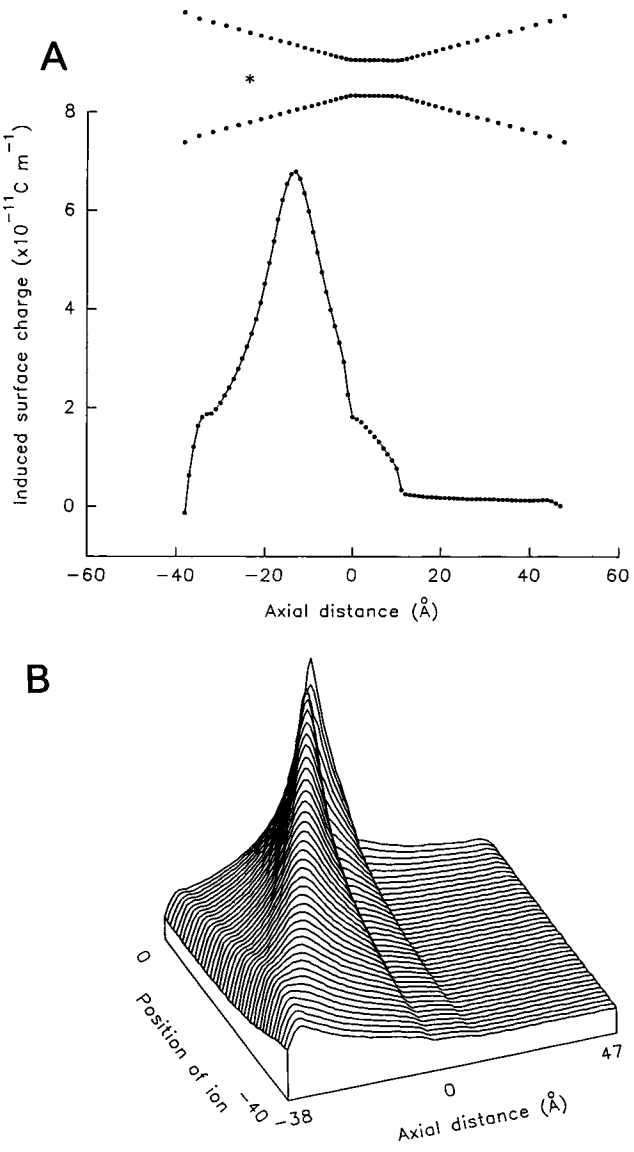

FIGURE 6 Induced surface charge density on the channel wall. These are the surface charges from the equivalent system described in Methods. (*a*) The magnitude of the induced surface charge on each circular ring in the channel wall is computed and then plotted against the axial distance. The inset shows the position of the ion in the vestibule, indicated with an asterisk in the outline of a 15° biconical channel. (*b*) A three-dimensional plot of the induced charge density is shown as the ion moves from the mouth of the vestibule (labeled −40 on the z axis) toward the constricted segment of the channel (labeled 0). The peak and the distribution of the induced surface charges change progressively as the ion moves into the channel.

Barrier height changes with conical angle

The magnitude of the potential barrier decreases systematically with increasing angle of the cone, as shown in Fig. 7 *a*. The four curves illustrated represent, from top to bottom, the conical angle of 10°, 20°, 40°, and 90°. The 90° biconical channel is similar to a gramicidin channel, if we assume that the dielectric constants of the lipid bilayer and the protein are about equal. A cation entering this pore

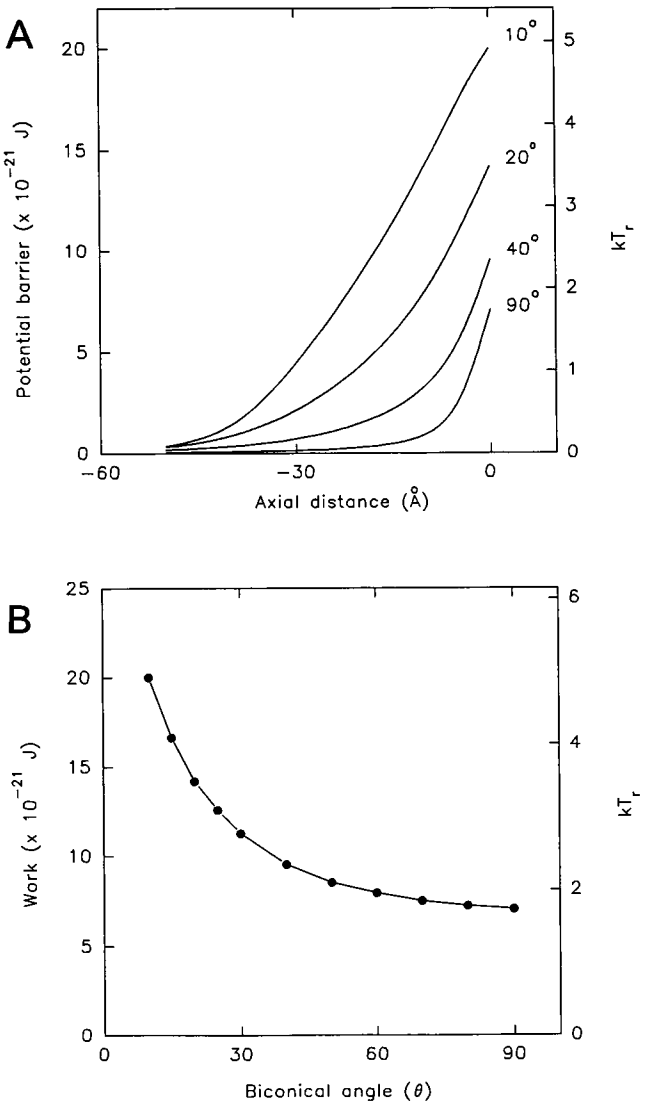

FIGURE 7 Reduction of the potential barrier with conical angle. (*a*) The potential barrier presented to the ion is systematically reduced as the angle of the cone becomes wider. The potential barrier determined for vestibules is plotted against axial distance. The number accompanying each curve is the conical angle in degrees. The energy unit given in kT_r in this and all subsequent figures refers to room temperature of 295°K. (*b*) The total amount of work required to move an ion from 10 Å beyond the top of the channel to the beginning of the constricted region is plotted against the conical angle. As the conical angle widens from 10° to 90°, the amount of work required decreases from 5 kT_r to 1.7 kT_r.

needs to surmount, in the absence of any anionic amino acid residue near the pore entrance, 1.7 kT_r of the energy barrier. (Throughout we will refer to the energy in room temperature units kT_r, where k is the Boltzmann constant and T_r is 295°K; 1 kT_r = 4.07 × 10^{-21} J = 2.45 kJ/mol). In contrast, the height of the energy barrier presented to the ion when the channel vestibule is a 10° cone reaches nearly 5 kT_r at the entrance of the constricted region, labeled 0 Å. In Fig. 7 *b*, the amount of work required to move an ion from the entrance of the vestibule to the narrow neck region of the channel, labeled as 0 Å, is plotted against the angle of the cone. The acuter the angle of the vestibule, the higher the energy barrier becomes, and thus the amount of work needed to transport an ion against the barrier increases steeply with decreasing conical angle. Note that we keep the side length of the cone fixed at 36 Å as we vary the angle, so that a decreasing angle implies a longer vestibule with a smaller radius at the mouth.

Dipoles are needed to cancel the barrier

To get an approximate idea of the effect of the repulsive force imposed on an ion by the vestibule, we have systematically applied a potential across the channel to counteract this force. A potential difference V is generated by applying a constant electric field along the z axis and adjusting the zero point and field strength until the electric potential is 0 at z = −50 Å and $-V$ at z = 60 Å. One such set of simulations is shown in Fig. 8 *a*, using a 15° biconical channel. The top curve, the potential barrier in the absence of an applied voltage, is reproduced from Fig. 4 *b*. The barrier height decreases steadily as the applied potential increases. To completely cancel the repulsive force experienced by an ion traversing the conical vestibule, it requires nearly 250 mV of electrical driving force across the channel.

Alternatively, the repulsive force can be counteracted by placing dipoles near the neck region of the channel. Fig. 8 *b* shows the systematic suppression of the potential barrier caused by placing dipoles on the protein wall of the constricted region. Four dipoles, positioned 90° apart and parallel to the z axis, are placed such that the negative charges are located at the beginning of the constricted region (labeled 0 Å in Fig. 4 *a*), and the positive charges 5 Å further inside. For computational convenience, the total dipole moments applied are varied by changing the amount of charge on each of the four dipoles. Because the dielectric constant for a charge at the boundary is not uniquely defined, we have used the average value for water and protein, which is equivalent to taking the sum of the charge and its image charge. The top curve in Fig. 8 *b*, the potential barrier in a 15° conical vestibule in the absence of any dipoles, is reproduced from Fig. 4 *a* and labeled as 0. The remaining four curves are, from top to bottom, the barrier heights obtained in the presence of dipoles, whose moments are 0.5, 1, 1.5, and 2 × 10^{-28} C m, respectively. (We note here that 1 Debye = 3.33 × 10^{-30} C m.) The barrier is completely eliminated when four dipoles with a total moment of 2 × 10^{-28} C m are used. This dipole strength is equivalent to two dipoles, each with a positive and a negative unit charge (1.6 × 10^{-19} C) separated by 6 Å. With two such dipoles, there is a small potential well of about 1.5 kT_r.

The vertical orientation of dipoles described above yields the maximum effect in the vestibule but is unrealistic, as the positive charges on the walls of the constricted region would completely block the channel to cations. A more likely scenario is that the dipoles are oriented 50–60° from the channel axis and are longer (8–10 Å), which would result in a similar potential.

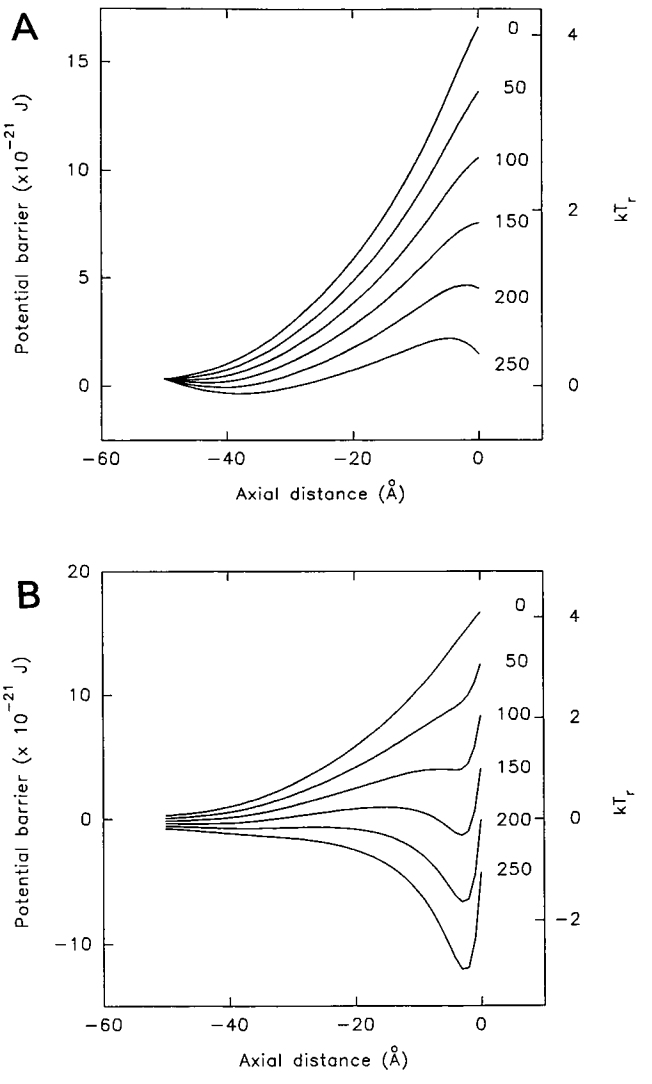

FIGURE 8 Electric potentials and dipole moments needed to counteract the repulsive image force. (*a*) The potential barrier presented to the ion by a 15° conical vestibule can be reduced by applying a potential difference across the channel. The energy barrier is plotted against axial distance with varying magnitude of the applied electric potential. The number accompanying each curve refers to the applied potential in millivolts. (*b*) The potential barrier presented to the ion by a 15° conical vestibule can be reduced by placing dipoles at the constricted region of the channel. The potential barrier is plotted against axial distance with varying moments of dipoles placed on the channel wall. The number accompanying each graph is dipole moments in units of $\times 10^{-30}$ C m.

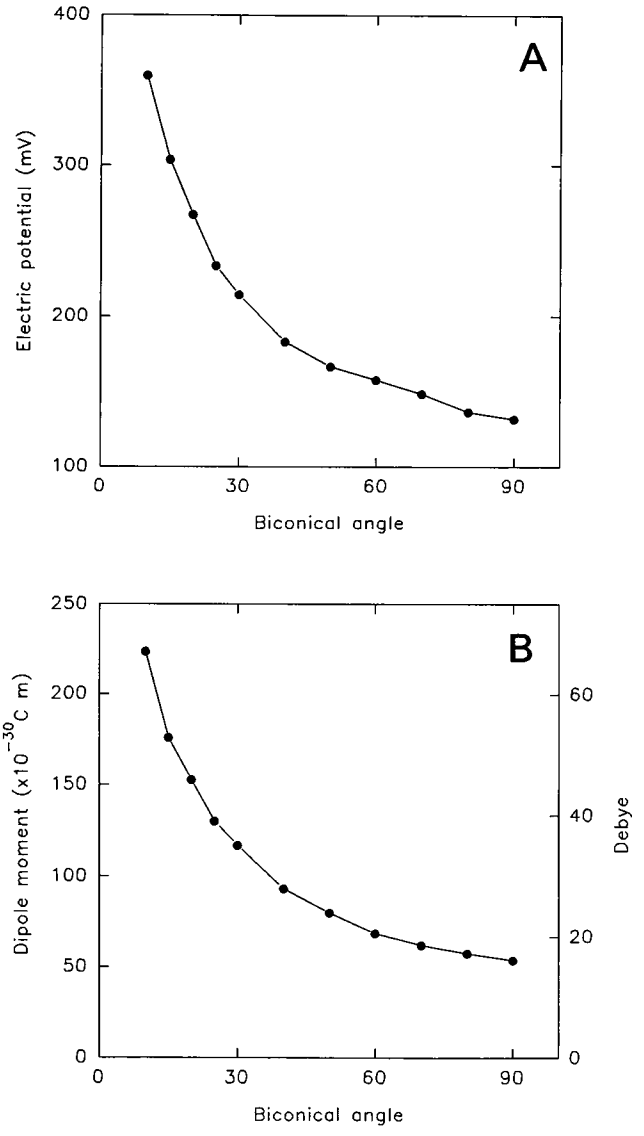

FIGURE 9 Electric potential and dipole moments needed to eliminate potential barrier from conical vestibules of varying angles. (*a*) The applied electric potential required to cancel the repulsive image force is plotted against conical angle. The values represent the electrical potential in millivolts required to reduce potential barrier everywhere in the vestibule to zero or less. (*b*) The dipole moment needed to eliminate the repulsive image force is plotted against the conical angle.

As one would have expected from the results illustrated in Fig. 7, the magnitude of the applied potential and of the dipole moments required to counteract the repulsive force decreases with the angle of the cone. The electric potential and dipole moment needed to eliminate the potential barrier in the vestibule are plotted against the angle of the cone in Fig. 9. For a gramicidin-like channel, the repulsive force presented to an ion by a planar lipid layer can be canceled by placing a dipole with a moment of about 16 Debyes near the entrance of the pore, assuming that the dielectric constant of the bilayer is the same as that of the protein.

Trajectory of the ion

The path of minimum resistance for an ion to penetrate the vestibule is the central axis. As the ion moves away from the central axis the potential barrier increases, at first gradually and then steeply as the ion approaches the vestibular wall to within 3 Å. This effect is shown in Fig. 10 *a* for the 15° biconical channel. The ion is moved 1.75 Å from the vestibular walls at the ends of each horizontal track. To reduce the errors, the grid size for this series of simulations is reduced to half of the usual spacing. The number accompanying each curve is the distance of the ion from the constricted region of the channel, in angstroms. As the vestibule

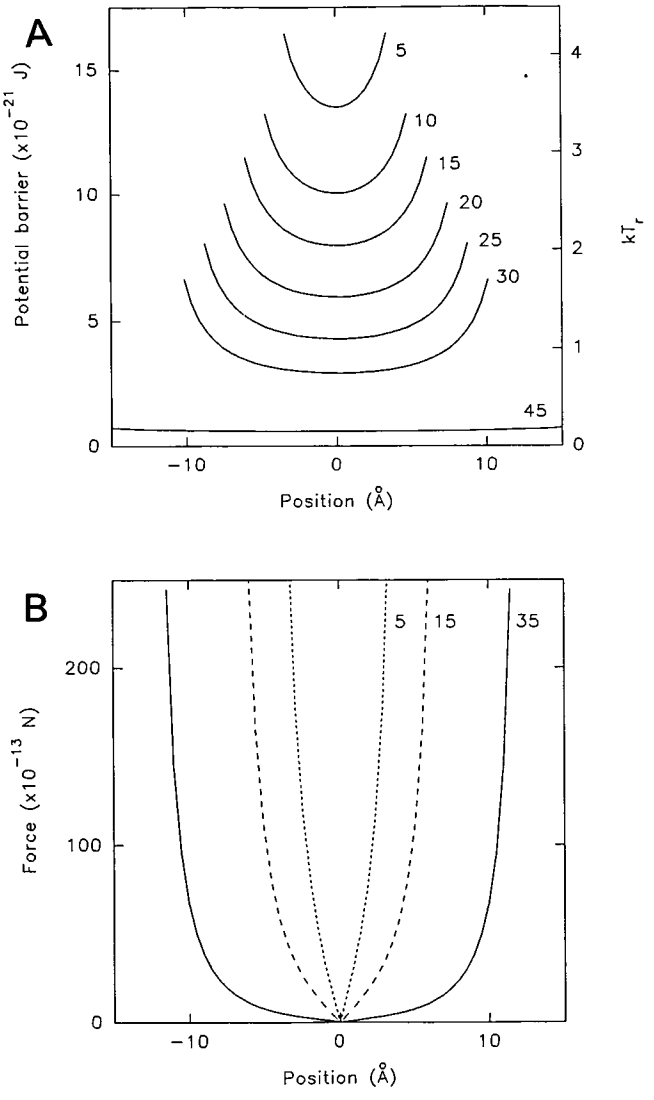

FIGURE 10 High potential barriers near the vestibular wall. (*a*) From a fixed position on the *z* axis of the vestibule, the ion is moved perpendicularly toward the vestibular wall, and the potential barrier is calculated at each vertical position. The number accompanying each curve refers to the distance in ångstroms from the beginning of the constricted channel region. (*b*) The magnitude of force on the ion directed toward the *z* axis is plotted at three different positions in the vestibule, as indicated by the numbers accompanying the curves. As the ion approaches the wall, this lateral force increases steeply, thus restricting the ion near the central axis as the vestibule narrows.

narrows the ion is confined to a decreasing region around the central axis. This is clearly shown in Fig. 10 *b*, in which the magnitude of force on the ion directed toward the *z* axis is plotted. Again, the numbers accompanying the curve represent the distance of the ion from the constricted region of the channel.

Effects of excess dipoles

In the previous section, we showed that the repulsive force resulting from induced charges can be canceled by a dipole moment of about 50 Debyes in the neck region (see Fig. 8 *b*). It is of interest to see the effect of excess dipoles on the distribution of ionic species in electrolyte solutions.

To investigate the effect of excess dipoles on the potential profile in the vestibule, we place four dipoles in the neck region. The total strength of the dipoles is 96 Debyes, nearly twice that needed to counteract the repulsive image force. Fig. 11 *a* shows the electric potential produced by the

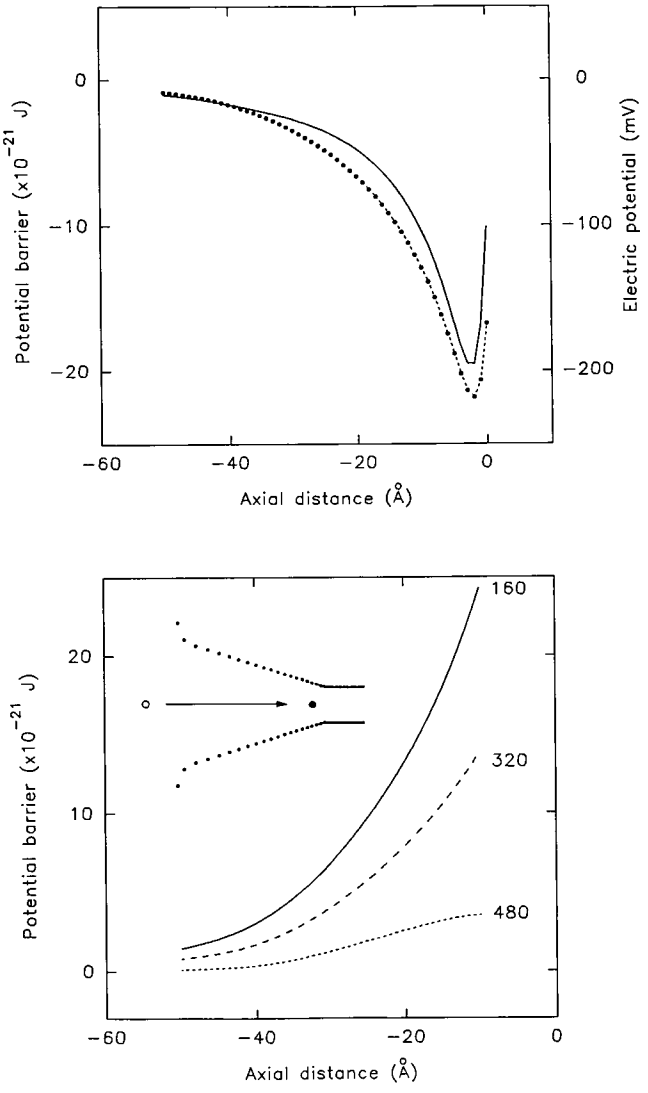

FIGURE 11 Attractive potentials created by excess dipoles. (*a*) Dipoles with a total moment of 96 Debyes, nearly twice that required to cancel the repulsive image force, are placed on the walls of the constricted region. The potential energy (*solid line*) and electric potential (*broken line*) created by these dipoles, the dielectric boundary, and, in the case of the potential barrier, a monovalent cation are plotted against axial distance. The potential well rapidly decays with distance from the location of the dipoles. (*b*) The potential barrier presented to a second ion entering the vestibule, given that one ion already is located in the region of maximum potential well, is plotted against axial distance. In the inset, the location of the first ion (*filled circle*) and the trajectory of the second ion (*open circle* and *arrow*) are schematically shown. The second ion is allowed to approach the first ion within a distance of 10 Å. The number accompanying each curve is the moment of the dipoles ($\times 10^{-30}$ C m) placed in the constricted region.

dipoles and dielectric boundary in the absence of any cations (*broken line*). It also shows attractive energy well felt by a monovalent cation in the vestibule due to the dipoles (*solid line*); this includes the image repulsion. There is an energy well of about 5 kT_r near the entrance of the constricted segment. The attractive potential decays nearly exponentially and reaches the $1/e$ value at a distance of 10 Å from this maximum. Clearly, there will be an increased probability of finding an ion in the region of the maximum attractive potential.

However, even in the presence of such an energy well, the probability of finding two cations in the vestibule is not appreciably increased. Fig. 11 *b* shows the energy barrier seen by the second ion as it enters the vestibule, given that the first ion is already confined in the potential well. In the inset, the position of the first ion (*filled circle*) and the trajectory of the second ion (*open circle* and *solid line*) are indicated schematically. When the moment of dipoles in the neck is 48 Debyes, just sufficient to cancel the repulsive force, the height of the energy barrier presented to the second ion increases to about 6 kT_r as it comes within 10 Å of the first ion (*solid line*). The barrier height halves when the moment of dipoles is increased to 96 Debyes (*dashed line*). It is only when the dipole moment is tripled to 144 Debyes that the potential barrier presented to the second ion in the vestibule disappears (*broken line*), and the mean distance between the two ions inside the vestibule becomes similar to that in bulk electrolyte solutions.

Because some biological ion channels are permeable to calcium, it is relevant to investigate the magnitude of repulsive force and the height of energy barrier presented to a divalent ion. The two curves shown in Fig. 12 *a* are calculated in the same way as those illustrated previously (Fig. 4), except that the ion carries two elementary charges. The barrier height and repulsive force for a divalent ion are four times, not twice, those for a monovalent ion. However, as shown in Fig. 12 *b*, the image force experienced by the divalent ion can be nearly canceled by the total dipole moment of about 100 Debyes, twice that required to have the same effect on a monovalent ion.

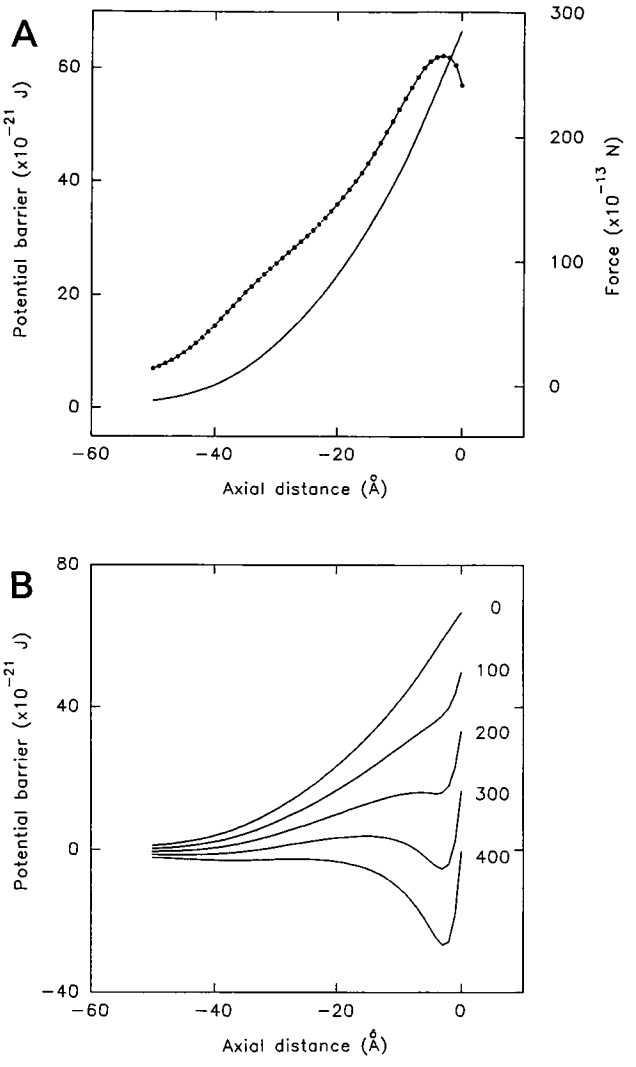

FIGURE 12 The potential barrier and repulsive image force presented to a divalent ion by a 15° conical vestibule. (*a*) The potential barrier (*solid line*) and repulsive force (*filled circles*) presented to a divalent ion are plotted against axial distance. The magnitudes of the barrier and of repulsive force are four times those presented to a monovalent ion (cf. Fig. 4). (*b*) The potential barriers in the presence of dipoles of varying moments are plotted against axial distance. The number accompanying each curve is the moment ($\times 10^{-30}$ C m) of dipoles positioned at the constricted channel region. The minimum dipole moment required to cancel the repulsive image force is twice that required for a monovalent ion (cf. Fig. 8).

DISCUSSION

Using the iterative method described above, we have determined the heights of the energy barriers presented to an ion by conical vestibules with an angle of 10° to 90° as well as a catenary vestibule. Levitt (1991a,b) proposed a theoretical scheme for calculating channel conductances from potential energy profiles using a modified Nernst-Planck equation. By combining our iterative method of deducing a potential profile for any arbitrarily shaped channel with Levitt's analytical method, it should now be possible to make testable predictions about how channel conductance will vary with various channel configurations. One conclusion emerging from our simulations is that the height of the potential barrier presented to an ion by the dielectric boundary of the vestibular wall is large compared to the ion's average kinetic energy. The peak height at the bottom of the vestibule, when the conical angle is, for example, 15°, is about 4 kT_r (Fig. 7). It requires nearly 250 mV of applied electric potential to drive the ion against such a barrier (Fig. 8). The probability that an ion entering the vestibule can successfully surmount a potential barrier of height V can be calculated using either simple statistical mechanics (Kuyucak and Chung, 1994) or the continuum equation (Dani and Levitt, 1990), or more rigorously by using the Fokker-Planck equation (Cooper et al., 1988). All of the

methods basically give the Boltzmann factor e^{-V/kT_r}; thus, the probability of transmission across such a barrier is rather low ($e^{-4} = 0.018$). We note that the constricted segment of the channel will present a further barrier to passage of ions, reducing the above probability even more.

Because of this barrier the presence of charged groups in the vestibule is a prerequisite for the free passage of an ion through the channel. If the vestibule in the ion channel has indeed shape and dimensions similar to those given by Toyoshima and Unwin (1988), then the repulsive force due to the charges on the vestibular wall will severely restrict transport of an ion unless several charged residues are placed near the channel's constricted region. The current across the channel, in the absence of such charge groups, will be attenuated by a factor of around 55. The number of charge groups required to eliminate the potential barrier depends on several factors. Among these are the location of counter charges (or the orientation and the strength of dipole moments) and the exact shape of the vestibule. In our calculation, it was assumed, for simplicity, that the dipoles are oriented parallel to the z axis, with the negative charge pointing to the mouth of the vestibule. With this assumption, the dipole moment needed to cancel the repulsive force on the ion is 1.75×10^{-28} C m (or $\sim$ 50 Debyes) for a 15° conical vestibule (Fig. 9). This is the minimum moment required; if the orientations of the dipoles are not perfectly parallel, the total moment required will be greater.

It is apparent that the selectivity of anions and cations can result from the polarity of charge groups or the orientation of dipoles located in the vestibule. For cationic channels, negative charges must be nearest to the entrance of the vestibule, whereas for anionic channels, positive charges must be closer. That the channel is permeable to a cation only when several dipoles are pointing away from it and impermeable otherwise raises an intriguing possibility that the passage or blockage of the ion could be controlled by a field-effect gate. This is one of the several possible mechanisms considered by Hille (1992) by which the channel may open and close. In principle, the gating could be controlled by the rotation of several dipoles, and the function of the vestibules might be to reduce leakage when the channel was closed, but whether such a mechanism operates in real biological channels remains to be investigated.

It is possible that there are more charged residues near the constricted region of the channel than the minimum number required to counteract the repulsive image force presented to the ion by the vestibule. The results of our simulation reveal that the presence of excess dipoles will have the effect of concentrating ions in the vestibule in the sense of increasing the probability of finding an ion in the small volume near the constricted region (see also Jordan, 1987). However, excess dipoles will not concentrate ions in the sense of attracting many ions into the vestibule, so that the concentration throughout the vestibule is significantly higher than that in the bulk solution. When there are twice as many dipoles as the minimum required, a potential barrier of about 3 kT_r is presented to a second ion that comes within 10 Å of the first ion. With three times as many dipoles, the repulsive interaction between the two ions in the vestibule disappears, and the mean distance between the ions will be kept at the Debye length, as in bulk electrolyte solutions (Fig. 11). The precise effect the excess charge groups will have on the conductance of single channels can be revealed by detailed calculations involving the Brownian dynamics method. The dependence or independence of conductance on the number of charged groups in the vestibule is an important point for further exploration. What is clear from our studies, however, is that a channel will become permeable to divalent ions if there are about twice as many dipoles as the minimum required. This fact may prove to be a valuable guide in determining the tertiary structure of the channel from its primary amino acid sequence.

It must be emphasized that conclusions drawn or inferences made from electrostatics are valid only in regions that are large compared to the diameters of water and ion molecules. Calculations involving dielectric constants and interactions between point charges describe the behavior of particles at the macroscopic level. In the channel region where the radius is less than 4 $\sim$ 5 Å, the dielectric constant falls off very fast with decreasing radius. This is the region of the nearest-neighbor water molecules, in which the representation of the dielectric as a continuous medium is a very poor approximation. For this reason, we have not attempted to calculate the potential profile inside of the constricted segment of the channel or attempted to estimate what the dielectric constant in it might be (cf. Monoi, 1991). Clearly, molecular dynamics calculations such as those reported for the gramicidin channel (e.g., Mackay et al., 1984; Roux and Karplus, 1991; Chiu et al., 1989) will be needed to elucidate the permeation process inside this region. By the same token, the values quoted for the dipole moments in the neck region should be taken as macroscopic estimates that require further microscopic studies.

APPENDIX A: SOLUTION OF ELECTROSTATIC POTENTIAL FOR A PROLATE BOUNDARY

Here we present the analytical solution for a point charge outside a prolate spheroid, the coordinate system of which is shown in Fig. 13. The charge q is in a dielectric medium with constant ε_1, and the spheroid has a dielectric constant ε_2. The surface of a prolate spheroid is defined by the relation $r_1 + r_2 =$ constant, where r_1 and r_2 are the distances from the two focuses of the spheroid

$$r_1 = [x^2 + y^2 + (z - a/2)^2]^{1/2},$$
$$r_2 = [x^2 + y^2 + (z + a/2)^2]^{1/2}. \tag{20}$$

The prolate spheroid coordinates $\{\xi, \eta, \phi\}$ are defined as

$$\xi = (r_1 + r_2)/a, \quad \eta = (r_1 - r_2)/a, \quad \tan\phi = x/y. \tag{21}$$

Here ξ has the range $[1, \infty]$ and measures the size of the spheroid in units of a. The orthogonal coordinates η and ϕ have the ranges $[-1, 1]$ and

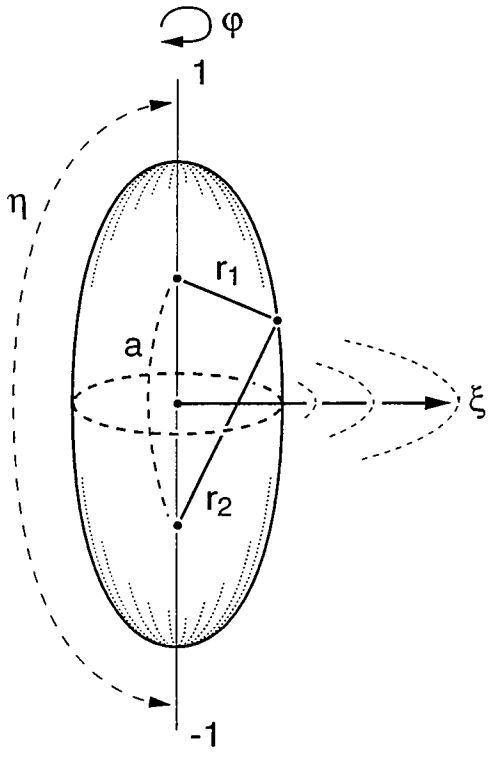

FIGURE 13 The coordinate system for a prolate spheroid. Three variables, ϕ, η, and ξ, define points everywhere in the space.

$[0, 2\pi]$, respectively. Inverse relations are

$$x = \frac{a}{2}[(\xi^2 - 1)(1 - \eta^2)]^{1/2}\cos\phi,$$

$$y = \frac{a}{2}[(\xi^2 - 1)(1 - \eta^2)]^{1/2}\sin\phi, \qquad z = \frac{a}{2}\xi\eta. \tag{22}$$

Solution of the Laplace equation is given in terms of the Legendre functions P_n^m, Q_n^m and $\cos m\phi$, $\sin m\phi$. Because Q_n^m diverges near zero, the η solution has only P_n^m, whereas the ξ solution could have either, depending on the boundary (Morse and Feshbach, 1953). Thus the most general potential can be written in the form

$$\varphi = \sum_{n=0}^{\infty}\sum_{m=0}^{m}[A_{nm}P_n^m(\xi) + B_{nm}Q_n^m(\xi)] \times P_n^m(\eta)[A'_{nm}\cos m\phi + B'_{nm}\sin m\phi], \tag{23}$$

where various constants (A's and B's) are to be determined from the boundary conditions. Potential due to a point charge q at ξ_0, η_0, ϕ_0 ($\xi_0 > \xi_1$) is given by Morse and Feshbach (1953) as

$$\varphi_p = \sum_{n=0}^{\infty}\sum_{m=0}^{n} C_{nm}\cos m(\phi - \phi_0)P_n^m(\eta_0)P_n^m(\eta) \times \begin{cases} P_n^m(\xi_0)Q_n^m(\xi) & \xi > \xi_0 \\ P_n^m(\xi)Q_n^m(\xi_0) & \xi < \xi_0 \end{cases}, \tag{24}$$

with

$$C_{nm} = \frac{q}{2\pi\varepsilon_0 a}(2n + 1)(2 - \delta_{m0})i^m\left[\frac{(n - m)!}{(n + m)!}\right]^2. \tag{25}$$

Superposing the two solutions and noting that, first, in Eq. 23, $B_{nm} = 0$ inside the boundary ($\xi < \xi_1$) and $A_{nm} = 0$ outside ($\xi > \xi_1$), and second, the ϕ solution in Eq. 23 must have the same form as in Eq. 24, we have for $\xi < \xi_0$

$$\varphi_{in} = \sum_{nm} A_{nm}P_n^m(\xi)P_n^m(\eta)\cos m(\phi - \phi_0),$$

$$\varphi_{out} = \frac{1}{\varepsilon_1}\sum_{nm}[B_{nm}Q_{nm}(\xi) + C_{nm}P_n^m(\eta_0)Q_n^m(\xi_0)P_n^m(\xi)] \times P_n^m(\eta)\cos m(\phi - \phi_0). \tag{26}$$

Because $P_n^m(\eta)$ and $\cos m(\phi - \phi_0)$ factor out, continuity of $\partial\varphi/\partial\eta$ and $\partial\varphi/\partial\phi$ implies $\varphi_{in} = \varphi_{out}$ at $\xi = \xi_1$. Thus,

$$\varepsilon_1 A_{nm}P_n^m(\xi_1) = B_{nm}Q_n^m(\xi_1) + C_{nm}P_n^m(\eta_0)Q_n^m(\xi_0)P_n^m(\xi_1). \tag{27}$$

The normal derivatives must satisfy

$$\varepsilon_2\frac{\partial\varphi_{in}}{\partial\xi}\bigg|_{\xi_1} = \varepsilon_1\frac{\partial\varphi_{out}}{\partial\xi}\bigg|_{\xi_1}, \tag{28}$$

yielding

$$\varepsilon_2 A_{nm}P_n^{m'}(\xi_1) = B_{nm}Q_n^{m'}(\xi_1) + C_{nm}P_n^m(\eta_0)Q_n^m(\xi_0)P_n^{m'}(\xi_1). \tag{29}$$

Solving Eqs. 28 and 29, we obtain

$$A_{nm} = \frac{Q_n^mP_n^{m'} - Q_n^{m'}P_n^m}{\varepsilon_2Q_n^mP_n^{m'} - \varepsilon_1Q_n^{m'}P_n^m}\bigg|_{\xi_1} P_n^m(\eta_0)Q_n^m(\xi_0)C_{nm},$$

$$B_{nm} = \frac{(\varepsilon_1 - \varepsilon_2)P_n^mP_n^{m'}}{\varepsilon_2Q_n^mP_n^{m'} - \varepsilon_1Q_n^{m'}P_n^m}\bigg|_{\xi_1} P_n^m(\eta_0)Q_n^m(\xi_0)C_{nm}. \tag{30}$$

Here the primes denote derivatives, which are given by

$$P_n^{m'} = \frac{1}{1 - \xi^2}[(n + 1)\xi P_n^m - (n - m + 1)P_{n+1}^m], \tag{31}$$

with an identical expression for $Q_n^{m'}$. The potentials are obtained upon substituting Eq. 30 in Eq. 26. A few simple checks on the solutions are provided in the limiting cases. For a conducting ellipsoid, $\varepsilon_2 \to \infty$, and A_{nm} in Eq. 30 and hence φ_{in} vanish. For $\varepsilon_1 = \varepsilon_2$, $B_{nm} = 0$ in Eq. 30, and the solutions reproduce the point charge potential (Eq. 24) everywhere.

APPENDIX B: SOLUTION OF ELECTROSTATIC POTENTIAL FOR THREE DIELECTRIC SLABS

Here we solve the three dielectric layers problem in a plane geometry. The results are used in addressing the effects of the sharp boundary assumption used in the calculation of channel potentials. Let t be the thickness of the middle layer, its center being located at the distance d from the charge. Assuming that the charge is at the origin and the plane boundaries separating the three layers (with dielectric constants ε_1, ε_2, ε_3) are at $z = d - t/2$ and $z = d + t/2$, the solutions for the electrostatic potentials in the three

regions can be written as

$$\varphi_1 = \frac{1}{4\pi\varepsilon_0}\int_0^\infty \left(\frac{q}{\varepsilon_1}e^{-kz} + f_1 e^{kz}\right) J_0(k\rho)\,dk, \qquad 0 < z < d - t/2,$$

$$\varphi_2 = \frac{1}{4\pi\varepsilon_0}\int_0^\infty (g_2 e^{-kz} + f_2 e^{kz}) J_0(k\rho)\,dk, \qquad d - t/2 < z < d + t/2, \tag{32}$$

$$\varphi_3 = \frac{1}{4\pi\varepsilon_0}\int_0^\infty g_3 e^{-kz} J_0(k\rho)\,dk, \quad d + t/2 < z,$$

where $J_0(k\rho)$ is the Bessel function of the first kind, order 0, and f_1, f_2, g_2, g_3 are unknown functions of k. Applying the usual boundary conditions at $z = d \pm t/2$, we obtain the following four equations for the four unknown functions

$$\begin{aligned}
\frac{q}{\varepsilon_1} + f_1 e^{k(2d-t)} &= g_2 + f_2 e^{k(2d-t)} \\
\varepsilon_1\left(-\frac{q}{\varepsilon_1} + f_1 e^{k(2d-t)}\right) &= \varepsilon_2(-g_2 + f_2 e^{k(2d-t)}) \\
g_2 + f_2 e^{k(2d+t)} &= g_3 \\
\varepsilon_2(-g_2 + f_2 e^{k(2d+t)}) &= -\varepsilon_3 g_3.
\end{aligned} \tag{33}$$

Solving Eq. 33, we obtain for f_1

$$f_1 = \frac{q}{\varepsilon_1}\left[\frac{(\varepsilon_1 - \varepsilon_2)(\varepsilon_2 + \varepsilon_3)e^{kt} + (\varepsilon_1 + \varepsilon_2)(\varepsilon_2 - \varepsilon_3)e^{-kt}}{(\varepsilon_1 + \varepsilon_2)(\varepsilon_2 + \varepsilon_3) + (\varepsilon_1 - \varepsilon_2)(\varepsilon_2 - \varepsilon_3)e^{-2kt}}\right]e^{-2kd}. \tag{34}$$

The integral of f_1 directly gives the potential acting on the charge due to the induced charges on the boundaries

$$\varphi_1(\mathbf{r} = 0) = \frac{1}{4\pi\varepsilon_0}\int_0^\infty f_1\,dk. \tag{35}$$

The integrals in Eqs. 34 and 35 are standard and are given by

$$\begin{aligned}
\int_0^\infty \frac{e^{-ak}}{c + e^{-bk}}\,dk &= \frac{1}{ac}\,{}_2F_1(1, a/b; 1 + a/b; -1/c), \\
&= \frac{1}{c}\sum_{n=0}^{\infty}\frac{(-1/c)^n}{a + nb},
\end{aligned} \tag{36}$$

where ${}_2F_1$ is a hypergeometric function and

$$a = 2d \pm t, \qquad b = 2t, \qquad c = \frac{(\varepsilon_1 + \varepsilon_2)(\varepsilon_2 + \varepsilon_3)}{(\varepsilon_1 - \varepsilon_2)(\varepsilon_2 - \varepsilon_3)}. \tag{37}$$

Using these results in Eqs. 34 and 35, we obtain for the potential

$$\varphi_1(\mathbf{r} = 0) = \frac{1}{4\pi\varepsilon_0}\frac{q}{\varepsilon_1}\sum_{n=0}^{\infty}\left[\frac{\varepsilon_1 - \varepsilon_2}{\varepsilon_1 + \varepsilon_2}\frac{(-1/c)^n}{2d + (2n-1)t} + \frac{\varepsilon_2 - \varepsilon_3}{\varepsilon_2 + \varepsilon_3}\frac{(-1/c)^n}{2d + (2n+1)t}\right]. \tag{38}$$

The terms in the summation correspond to multiple image charges similar to multiple reflections in parallel mirrors.

The potential plotted as a function of the distance from the protein-water interface in Fig. 3 is calculated from Eq. 38.

The calculations upon which this work is based were carried out using the Fujitsu VP 2200 of the ANU Supercomputer Facility. Throughout the course of this study, Sarah Lendon has provided excellent technical assistance, for which we are grateful.

This work was supported by grants from the Australian Research Council and the National Health and Medical Research Council of Australia.

REFERENCES

Chiu, S.-W., S. Subramaniam, E. Jakobsson, and J. A. McCammon. 1989. Water and polypeptide conformations in the gramicidin channel. *Biophys. J.* 56:253–261.

Cooper, K. E., P. Y. Gates, and R. S. Eisenberg. 1988. Surmounting barriers in ionic channels. *Q. Rev. Biophys.* 21:331–364.

Dani, J. A., and D. G. Levitt. 1990. Diffusion and kinetic approaches to describe permeation in ionic channels. *J. Theor. Biol.* 146:289–301.

Hille, B. 1992. Ionic Channels of Excitable Membranes. Sinauer Associates, Sunderland, MA.

Jordan, P. C. 1981. Energy barriers for passage of ions through channels. Exact solution of two electrostatic problems. *Biophys. Chem.* 13: 203–212.

Jordan, P. C. 1982. Electrostatic modeling of ion pores. Energy barriers and electric field profiles. *Biophys. J.* 39:157–164.

Jordan, P. C. 1983. Electrostatic modeling of ion pores. II. Effects attributable to the membrane dipole potential. *Biophys. J.* 41:189–195.

Jordan, P. C. 1984a. Effect of pore structure on energy barriers and applied voltage profiles. I. Symmetrical channels. *Biophys. J.* 45:1091–1100.

Jordan, P. C. 1984b. Effect of pore structure on energy barriers and applied voltage profiles. II. Unsymmetrical channels. *Biophys. J.* 45:1101–1107.

Jordan, P. C. 1987. How pore mouth charge distributions alter the permeability of transmembrane ionic channels. *Biophys. J.* 51:297–311.

Jordan, P. C., R. J. Bacquet, J. A. McCammon, and P. Tran. 1989. How electrolyte shielding influences the electrical potential in transmembrane ion channels. *Biophys. J.* 55:1041–1052.

Kuyucak, S., and S. H. Chung. 1994. Temperature dependence of conductivity in electrolyte solutions and ionic channels of biological membranes. *Biophys. Chem.* 52:15–24.

Levitt, D. G. 1978a. Electrostatic calculations for an ion channel. I. Energy and potential profiles and interactions between ions. *Biophys. J.* 22: 209–219.

Levitt, D. G. 1978b. Electrostatic calculations for an ion channel. II. Kinetic behavior of the gramicidin A channel. *Biophys. J.* 22:221–248.

Levitt, D. G. 1991a. General continuum theory for multiion channel. I. Theory. *Biophys. J.* 59:271–277.

Levitt, D. G. 1991b. General continuum theory for multiion channel. II. Application to acetylcholine channel. *Biophys. J.* 59:278–288.

Mackay, D. H. J., P. H. Berens, K. R. Wilson, and A. T. Hagler. 1984. Structure and dynamics of ion transport through gramicidin A. *Biophys. J.* 46:229–248.

Monoi, H. 1991. Effective pore radius of the gramicidin channel. Electrostatic energies of ions calculated by a three-dielectric model. *Biophys. J.* 59:786–794.

Morse, P. M., and H. Feshbach. 1953. Methods of Theoretical Physics, Vol. II. McGraw-Hill, New York.

Parsegian, A. 1969. Energy of an ion crossing a low dielectric membrane: solutions to four relevant electrostatic problems. *Nature.* 221:844–846.

Roux, B., and M. Karplus. 1991. Ion transport in a model gramicidin channel: structure and thermodynamics. *Biophys. J.* 59:961–981.

Toyoshima, C., and N. Unwin. 1988. Ion channel of acetylcholine receptor reconstructed from images of postsynaptic membranes. *Nature.* 336: 247–250.

Unwin, N. 1989. The structure of ion channels in membranes of excitable cells. *Neuron.* 3:665–676.

Unwin, N. 1995. Acetylcholine receptor channel imaged in the open state. *Nature.* 373:37–43.